

HOMOLOGOUS JET-DRIVEN CORONAL MASS EJECTIONS FROM SOLAR ACTIVE REGION 12192

NAVDEEP K. PANESAR^{1,2}, ALPHONSE C. STERLING¹, RONALD L. MOORE^{1,2}

¹Heliophysics and Planetary Science Office, ZP13, Marshall Space Flight Center, Huntsville, AL
35812, USA and

²Center for Space Plasma and Aeronomic Research (CSPAR), UAH, Huntsville, AL
35805, USA

Draft version March 6, 2022

ABSTRACT

We report observations of homologous coronal jets and their coronal mass ejections (CMEs) observed by instruments onboard the *Solar Dynamics Observatory (SDO)* and *Solar and Heliospheric Observatory (SOHO)* spacecraft. The homologous jets originated from a location with emerging and canceling magnetic field at the southeast edge of the giant active region (AR) of 2014 October, NOAA 12192. This AR produced in its interior many non-jet major flare eruptions (X and M class) that made no CME. During 20-27 October, in contrast to the major-flare eruptions in the interior, six of the homologous jets from the edge resulted in CMEs. Each jet-driven CME ($\sim 200\text{-}300\text{ km s}^{-1}$) was slower-moving than most CMEs; had angular width ($20^\circ - 50^\circ$) comparable to that of the base of a coronal streamer straddling the AR; and was of the ‘streamer-puff’ variety, whereby the preexisting streamer was transiently inflated but not destroyed by the passage of the CME. Much of the transition-region-temperature plasma in the CME-producing jets escaped from the Sun, whereas relatively more of the transition-region plasma in non-CME-producing jets fell back to the solar surface. Also, the CME-producing jets tended to be faster and longer-lasting than the non-CME-producing jets. Our observations imply: each jet and CME resulted from reconnection opening of twisted field that erupted from the jet base; and the erupting field did not become a plasmoid as previously envisioned for streamer-puff CMEs, but instead the jet-guiding streamer-base loop was blown out by the loop’s twist from the reconnection.

Subject headings: Sun: activity — Sun: flares — Sun: coronal mass ejections (CMEs)

1. INTRODUCTION

Active region (AR) NOAA 12192 contained the largest sunspot group to date of solar cycle 24¹. The interior of this AR produced a multitude of big X-and M-class flares as well as many B- and C-class flares during its passage across the solar disk from 2014 October 17 to 30. All of these interior flares were confined, i.e. they did not produce CMEs (Thalmann et al. 2015; Sun et al. 2015; Chen et al. 2015). The AR apparently produced a large fast CME on October 14, before it rotated onto the disk (West & Seaton 2015). During disk passage, it produced six ‘streamer-puff CMEs’ (Bemporad et al. 2005), where the CME comes from a compact ejective eruption in a foot of one loop of a coronal-streamer base magnetic arcade and the streamer transiently bulges out but is not blown away completely by the passage of the CME (Moore & Sterling 2007; Jiang et al. 2009). Only one of these CMEs, accompanied by an M4.0 flare, was previously reported (Thalmann et al. 2015; Chen et al. 2015; Li et al. 2015). They all originated from the southeast edge of the AR, from a series of coronal jets occurring at a neutral-line-containing subregion at that location, a neutral line separate from that of the AR-interior confined flares.

“Jets” are dynamic, transient, collimated features that become long compared to their width. Those with coronal emissions (‘coronal jets’) occur in coronal holes, quiet regions, and ARs, and have a brightening at their base (e.g. Shibata et al. 1992; Shimojo et al. 1996; Sheeley et al. 1999; Cirtain et al. 2007; Nisticò et al. 2009). Our observed jets might also be referred to as “surges” (Zirin 1988). Jets are frequently described as occurring on open-field regions (coronal holes, or

at AR-coronal-hole boundaries), whereas our jets here occur on relatively-large-scale closed loops of an AR.

There are various definitions of CMEs (e.g. Sheeley et al. 2009; Vourlidas et al. 2013), here we use the term to mean a coronal ejection that is listed in the LASCO CME catalog².

In addition to the CME-producing jets, many other jets from the same subregion did not produce CMEs. Here we discuss the CMEs and the CME-producing jets, and differences between the CME-producing and the non-CMEs-producing jets. We then present our interpretation that the CMEs were driven by magnetic twist injected by the reconnection that made the CME-producing jets.

2. INSTRUMENTATION AND DATA

In our analysis we used EUV images and movies from the *Solar Dynamics Observatory (SDO)/Atmospheric Imaging Assembly (AIA)* to study the jets, and we used images from the C2 coronagraph of the *Large Angle and Spectrometric Coronagraph (LASCO; Brueckner et al. (1995))* onboard the *Solar and Heliospheric Observatory (SOHO)* to study the CMEs. LASCO/C2 shows the outer corona between $2 R_\odot$ and $6 R_\odot$ with a temporal cadence of 12 minutes (Brueckner et al. 1995).

The *SDO/AIA* images have a cadence of 12 s and spatial resolution of $0''.6\text{ pixel}^{-1}$ (Lemen et al. 2012). We used primarily 304 \AA and 193 \AA images³ to view transition-region-temperature and coronal-temperature jet structures. We derotated all the AIA images to a particular time and created movies with relatively coarse temporal cadence (of 1-minute), which was sufficient for studying the jets’ evolution.

navdeep.k.panesar@nasa.gov

¹ <http://www.thesuntoday.org/tag/sunspot/>

² http://cdaw.gsfc.nasa.gov/CME_list

³ <http://jsoc.stanford.edu/ajax/exportdata.html>

Table 1
Date and time for the observed jets, and their measured parameters.

a) CME-producing Jets:									
Jet No	Date (UT)	Time ^a	Flare class	CME Speed ^{b,c} (km s ⁻¹)	CME Angular width (°)	Jet Speed ^d (km s ⁻¹)	Jet Rise Dur. (± 5 min)	Jet Width ^e (± 1500 km)	Remote Bri.& Dim.
J1	20-Oct-14	18:43	C6.2	187	40	190 ± 10	20	34000	Yes
J2	22-Oct-14	16:52	C5.8	281	20	310 ± 20	30	38000	Yes
J3	23-Oct-14	19:11	C3.3	239	35	330 ± 20	50	26000	No
J4	24-Oct-14	03:56	C3.6	250	30	300 ± 20	45	34000	Yes
J5	24-Oct-14	07:37	M4.0	677	50	400 ± 40	35	86000	Yes
J6	27-Oct-14	17:33	M1.4	186	25	ambiguous ^f	-	-	- ^g
b) Non-CME-producing Jets:									
Jet No	Date (UT)	Time	Flare class	CME Speed	CME Angular width	Jet Speed	Jet Rise Dur.	Jet Width	Remote Bri.& Dim.
J8	22-Oct-14	02:31	-	-	-	75 ± 10	35	19000	-
J9	22-Oct-14	05:51	-	-	-	120 ± 20	10	15000	-
J10	22-Oct-14	10:46	C1.9	-	-	140 ± 20	15	11000	-
J11	22-Oct-14	12:56	-	-	-	50 ± 10	20	16500	-
J12	22-Oct-14	17:30	C3.0	-	-	ambiguous ^h	10	13000	-
J13	22-Oct-14	20:11	C3.0	-	-	150 ± 20	10	16000	-
J14	22-Oct-14	23:15	C1.1	-	-	110 ± 10	25	13000	-

^a<http://ftp.ngdc.noaa.gov/STP/space-weather/solar-data/solar-features/solar-flares/x-rays/goes/2014/>

^bhttp://cdaw.gsfc.nasa.gov/CME_list

^cThe uncertainty in the CMEs speed measurement is less than 10% (Yashiro et al. 2004).

^dThe uncertainties are estimated from the time-distance plots.

^eMeasured at a projected height of ~72000 km from jet base.

^fThis jet shows up well in the AIA 94 Å images, but not in 304 Å images. Due to its poor visibility in 304 Å images, we were unable to follow the jet plasma well enough to measure its speed.

^gAR was close to the west limb, obscuring any remote brightening/dimming.

^hSlower velocity (250 km s⁻¹) in the beginning, but faster (>650 km s⁻¹) later when a plug of plasma separates.

The X-ray Telescope (XRT) on *Hinode* had coverage of only three of our six CME-producing jets (J1, J2, and J5 in Table 1). Each of these three jets was clearly visible in the XRT images. So, probably all six of our CME-producing AIA jets were X-ray jets having cooler EUV components.

We studied the photospheric magnetic field using *SDO/Helioseismic and Magnetic Imager (HMI)*; Schou et al. (2012) line-of-sight magnetograms, which have cadence of 45 s and spatial resolution of 0''.5 pixel⁻¹ (Scherrer et al. 2012).

We found a total of six CME-producing homologous solar jets from AR NOAA 12192 between 2014 October 20 and 27. These ejective jets and CMEs were first identified by looking at movies from JHelioviewer⁴. Table 1(a) lists the six jets and corresponding CMEs. We also studied the properties of seven non-CME-producing jets of 2014 October 22; see Table 1(b).

3. OBSERVATIONS

Figure 3(c) shows the AR. The highly-dynamic jetting location is on the south edge of the AR (Figure 3(a)). This location produced six ejective eruptions, each of which produced a flare, jet and CME (Table 1(a)). These jets have characteristics of blowout jets (Moore et al. 2010). These eruptions were reported in the *Reuven Ramaty High-Energy Solar Spectroscopic Imager (RHESSI)*⁵; Lin et al. (2002) flare list, as well as in the *LASCO CME*⁶ and NOAA flare catalogs.⁷

3.1. Evolution of Jets and CMEs

⁴ <http://www.jhelioviewer.org>

⁵ http://hesperia.gsfc.nasa.gov/hessidata/dbase/hessi_flare_list.txt

⁶ http://cdaw.gsfc.nasa.gov/CME_list

⁷ <http://ftp.ngdc.noaa.gov/STP/space-weather/solar-data/solar-features/solar-flares/solar-flare-lists/2014/201410201410/>

Figure 1 shows three of the homologous jets observed by *SDO/AIA*. Figure 1(a-c) shows the progression of jet J2. The white arrows in Figure 1(a) point to brightenings in the base of the jet as the jet begins to rise. Later (in Figure 1(b)), the outward-moving jet spire extends higher in the corona (Figures 1(c) and 3(c)). The bright spire appears to extend along twisting magnetic field (e.g., at 16:58 UT in Figure 1(b), also see MOVIE304). The transverse-motion in Figures 3(d) and (f) (the insets) show definite twisting-motion tracks (traced by blue lines). The upper part of (304 Å) jet J2 leaves the AIA field of view (FOV) at ~17:21 UT (MOVIE304), showing that the material exceeded a height of 6.1×10^5 km (which is the plane-of-sky distance from the jet base to the edge of the AIA FOV along the jet's path). After that the lower part of the jet fades away slowly and some of the jet material falls back to the solar surface (~18:26 UT). Figures 1(e-g) and 1(i-k) respectively show example images of jets J4 and J5. We find that the jets recur and emanate from the same region, and have similar structure and development; that is, they are homologous (Dodson-Prince & Bruzek 1977).

Figures 1(d), (h), and (l) show the remote brightening and/or dimming at the other end of the loop during the jet eruptions. We discuss the brightenings in Section 4. The dimmings support that the loop is ejected as the CME. Such far-end brightenings and dimmings are not discernible in J3 (Table 1), but that event is weaker than the others.

In Figure 2(a-c), we show the CME corresponding to jet J2 (Figure 2(a) and MOVIECME). There is no indication of the CME (Figure 2(a)) while the jet is still in the AIA FOV. But as soon as the jet moves beyond the AIA FOV, the preexisting coronal streamer starts to inflate (see the non-difference *LASCO* movie⁸) as the CME is developing. Figure 2(b)

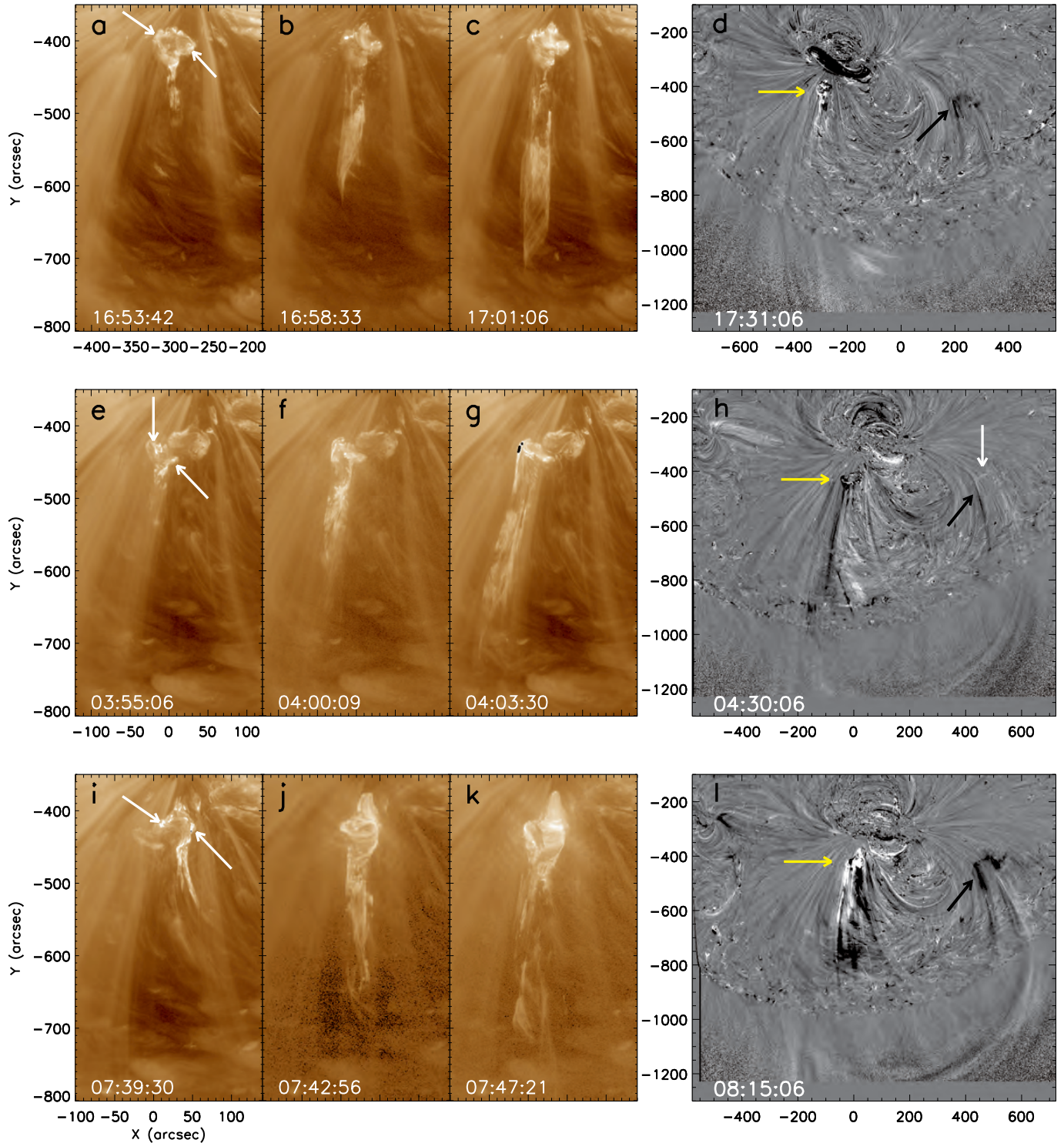


Figure 1. Evolution of homologous jets: AIA 193 Å intensity images of J2 (a-c), J4 (d-f), and J5 (g-i) of Table 1. In (a), (e), and (i), the arrows point to flare ribbons brightening in the jet base during the rise phase of the jet. Panels (d), (h), and (l) show AIA 193 Å base-difference images. The black and yellow arrows point to the remote dimmings and jet-origin region, respectively. The white arrow points to a remote brightening. Animations of (d), (h), and (l) are available online; white arrows in selected frames show brightenings.

shows the early phase of the CME when the jet was still escaping from the AIA FOV, and after that the CME continued to expand and escape, and definitely shows twisted structure and untwisting motion (MOVIECME). Our other streamer-puff CMEs show less definite evidence of twist in the LASCO C2 running-difference movies⁹. The streamer was not blown out by the passage of the CME, only disturbed (i.e., transiently inflated). Figures 2(d-f) and 2(g-i) respectively show the CMEs from jets J4 and J5. These jet-driven CMEs had relatively narrow angular width (20°- 50°; see Table 1(a)), comparable to that of the streamer base (~40°). The second CME observed on 2014 October 24 (from Jet J5) had the largest angular width (Figure 2(i)) of the CMEs of Table 1(a).

3.2. Jet and CME Speeds

All six CME-producing jets contain substantial transition-region (304 Å) emitting material. We measured the plane-of-sky speeds of the jets as they erupted and flowed outward (Table 1). We take a straight line along the main axis of the jet in 304 Å (Figure 3(c)) to construct a height-time plot. Figure 3(d) shows the plot for jet J2 along the white fiducial line in Figure 3(c). It shows a bright outward flow of plasma starting at ~ 16:52 UT. The total duration of this jet is about 30 minutes. Plasma was propelled high into the corona (Figure 3(d) and MOVIE304); only a small fraction appears to fall back to the solar surface, while most material flowed out of the AIA FOV (similarly the other five jets of Table 1(a) largely left the AIA FOV). The slope of the green dashed arrow in Figure 3(d) gives 310 km s^{-1} for the upflow speed of jet J2.

Figure 3(d) shows another enhanced brightening beginning at 17:32 UT, which is due to a subsequent jet that was not centered on the white line of Figure 3(c). This was a non-CME-producing jet (J12; Table 1(b)). One can see in MOVIE304 that plasma from this jet does not reach as high as the earlier jet (J2). The material of jet J12 mainly becomes trapped in closed field lines.

Figure 3(e) shows jet J5, the largest jet of our data set, which erupts in conjunction with an M4.0 flare. Figure 3(f) shows the height-time plot along the white fiducial line of Figure 3(e). This jet is much broader than other jets shown in Table 1(a), and had a plane-of-sky speed of about 400 km s^{-1} along the white line (slope of the green dashed arrow). This jet produced a CME with plane-of-the-sky speed of 680 km s^{-1} , which is twice that of the CME from jet J2. Speeds of all five jets and CMEs are listed in Table 1(a). The CME speeds are taken from the LASCO CME catalog. We extrapolated a linear fit of the plane-of-the-sky speeds back in time, and found the start times to match well with the jet start times for all six cases. This further supports that the CMEs originated from the jets.

To see the difference between the CME-producing jets and non-CME-producing jets, we measured the speeds, durations and widths of both categories of jets (Table 1(a,b)). Unlike the CME-producing jets, the non-CME jets do not show a clear/visible and traceable ejection of transition-region plasma leaving the AIA FOV. For calculating their outflow speeds, we tracked the leading edge of the jet in the 304 Å images during the jets' rise. (Using this method to measure speeds of the six CME-producing jets does not result in values substantially different from those listed in Table 1(a), which we found using the time-distance plots such as in Fig-

ures 3(d) and 3(f). Thus our two speed-measurement methods are mutually-consistent.) The non-CME jets that erupted in conjunction with substantial flares (J10, J12, J13 and J14) had higher speeds than the non-CME jets (J8, J9 and J11).

Figure 3(a) shows the underlying magnetic field of the AR and jet region. The jet base is a complex mix of emerging and canceling flux (Figure 3(b)) throughout the disk passage of AR 12192. Therefore we can only conclude that the jets occurred from a location where both flux emergence and cancellation were occurring. The properties of our jets are typical of those of *Yohkoh*/SXT-observed jets from ARs (Shimojō et al. 1996).

4. SUMMARY AND DISCUSSION

Our CME-producing jets have different properties than our non-CME-producing jets. We find the following: (a) relatively more of the cool transition-region plasma escaped from the Sun in the case of CME-producing jets whereas relatively more fell back to the surface in the non-CME-producing jets; (b) the CME-producing jets are faster ($300 \pm 75 \text{ km s}^{-1}$) than the non-CME-producing jets ($105 \pm 40 \text{ km s}^{-1}$); (c) they tend to be longer in duration (mean duration and weighted standard deviation are 35 and 10 minutes, respectively) than the non-CME-producing jets (18 and 9 minutes, respectively); and d) they are wider (mean width and weighted standard deviation are 43,000 and 24,000 km, respectively) than the non-CME-producing jets (15,000 and 27,00 km, respectively). Our jet-driven CMEs are slower (speed $\sim 300 \text{ km s}^{-1}$) than average CMEs with flares ($\geq 750 \text{ km s}^{-1}$, e.g. Sheeley et al. 1999).

Our CMEs result from jet eruptions. Recently, it has been found that jets in coronal holes are driven by minifilament eruptions (Sterling et al. 2015). The minifilaments reside in presumably-twisted magnetic field in the core of a small bipole between ambient open field and the minority-polarity side of a larger bipole. The minifilament-carrying bipole erupts and reconnects with the open field, producing the jet. It is plausible that our AR jets here operate the same way as Sterling et al. (2015) coronal hole jets (cf. Li et al. 2015). We further speculate that our jets lead to the CMEs as follows. During the reconnection, twist of the erupting-minifilament field is transferred to the newly-reconnected open field (Pariat et al. 2009; Török et al. 2009; Shibata & Uchida 1986; Archontis & Hood 2013; Fang et al. 2014; Moore et al. 2015). Since our AR jet eruptions occur in the foot of one loop of the streamer-base arcade, only that loop gets blown out rather than the whole arcade and whole streamer, and thus results in a streamer-puff CME (Bemporad et al. 2005).

Figure 4 shows a schematic of this proposed process based on our observations. The jet-producing region (dashed box in Figure 4(a)) is embedded in the outskirts of the overall arcade of loops of the AR and inside the arcade base of a LASCO-observed large streamer. Based on Sterling et al. (2015) and because there is cool transition-region plasma in our jets, we assume that the jet-producing region (Figures 4(a) and 4(a1)) includes a sheared field that contains a minifilament (Li et al. 2015 confirm that at least one of the jets of this region originates as an erupting (mini)filament). And since we observe spinning motion in our jets, we further assume that the minifilament resides in twisted field (e.g. Moore et al. 2015). Following the schematic of Sterling et al. (2015), we envision that at the start of the jet the minifilament-holding field erupts, and undergoes two forms of magnetic reconnection: (i) *internal reconnection* among the legs of field inside of (i.e. *internal* to) the erupting minifilament field (lowest star in Figure

⁹ http://cdaw.gsfc.nasa.gov/CME_list

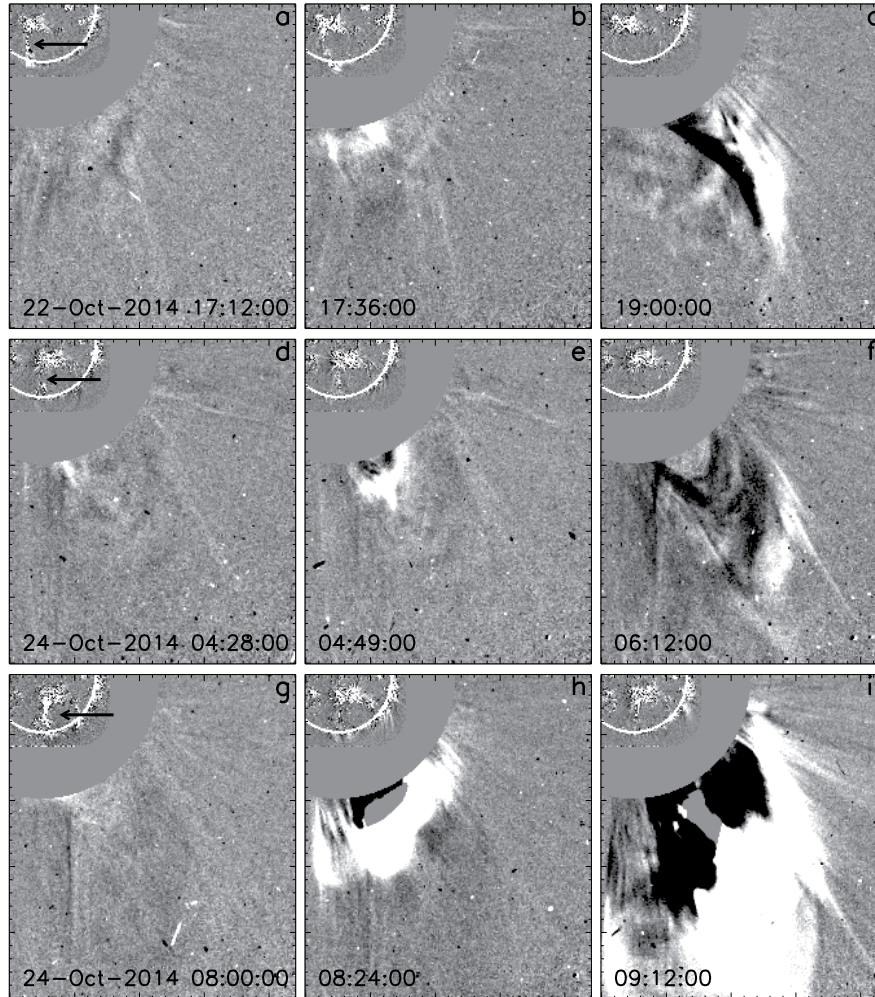


Figure 2. Progression of CMEs: (a-c), (d-f), and (g-i) are LASCO C2 running-difference images respectively showing the streamer-puff CMEs from jets J2, J4, and J5. In each frame, an *SDO/AIA* 193 Å running-difference image is co-aligned with the C2 image. The outer edge of the AIA solar disk is outlined in white in each frame. The black arrows in (a), (d) and (g) point to the J2, J4 and J5 jets, respectively. Animation of J2 (a-c) is available online.

4(a1)) that makes bright flare ribbons and loops at the jet base (shown as the jet-base left-hand-side small magenta loop in Figures 4(b) and 4(c)), and (ii) *external reconnection* (highest star in Figure 4(a1)) of the erupting minifilament field with a loop of the big arcade that is *external* to the minifilament field. This external reconnection: (1) makes the jet-base right-hand-side small magenta loop in Figures 4(b) and 4(c), and (2) transfers twist from the erupting field to the reconnecting big loop (red twisted lines in Figure 4(b)). We observed remote brightenings and dimmings at the far end of the erupting-CME loop (Figure 1(d), (h), and (l) and Table 1), consistent with this picture; the brightenings are from high-speed electrons that are accelerated by the external reconnection, escape along the big loop, and impact the far-end lower atmosphere (e.g. Tang & Moore 1982), and the dimmings are due to the big-loop blowout (e.g. Moore & Sterling 2007). During the eruptions, only one segment of the outer streamer arcade gets ejected rather than the whole coronal streamer arcade because the jet eruptions occur in the foot of only one loop of the arcade. The added magnetic pressure from the added twist drives the arcade loop out to become the streamer-puff CME; that is, the twist-loaded magnetic loop of

the streamer base (Figure 4(c)) erupts to become the streamer-puff CME. After each eruption, the opened field presumably recloses by reconnection, which allows the series of CMEs from the homologous jets (Sterling & Moore 2001; Panesar et al. 2015).

The non-CME-producing jets are weaker, and apparently do not transfer enough twist to the streamer-base loop to blow it out as a discernible streamer-puff CME.

This picture of streamer-puff CMEs differs from that of Bemporad et al. (2005). They proposed a scenario whereby a flux-rope plasmoid explodes up the leg of the loop of the streamer-base arcade from a compact ejective flare eruption, and explodes the loop top outward to become the streamer-puff CME (Bemporad et al. 2005; Moore & Sterling 2007; Jiang et al. 2009). We propose that the CMEs are driven by the helicity loaded onto the magnetic-arch loop from the erupting minifilament field as the jet forms, rather than by an erupting plasmoid as suggested by Bemporad et al. (2005).

High-quality AIA data were not available for the events of Bemporad et al. (2005). We have since learned that many jets result from minifilament eruptions (Sterling et al. 2015), and so we suspect the jets we observe here occur that way

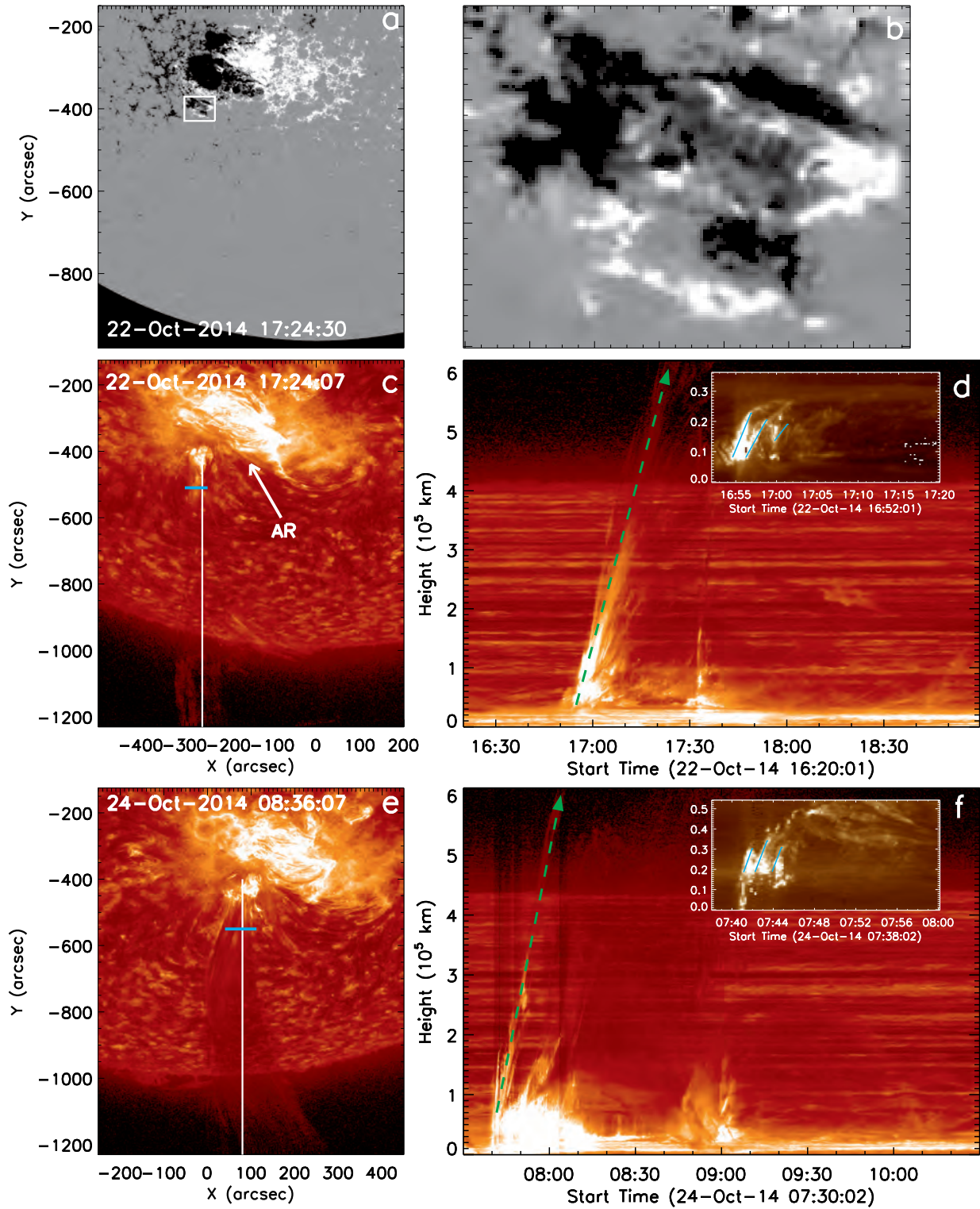


Figure 3. Jet outflow and spin: (a) HMI line-of-sight magnetogram of AR 12192 (b) The jet-producing region (white box of a). (c) AIA 304 Å intensity image of jet J2, and (e) jet J5 of Table 1. The white lines in (c) and (e) mark the positions of the time-distance plots in (d) and (f), respectively. Panels (d) and (f) show AIA 304 Å intensity height-time-series images along the vertical lines in panel (c) and (e), respectively. Insets in (d) and (f) show the 193 Å intensity time-series images along the blue lines in panel (c) and (e), respectively; they show changes consistent with jet twisting with time. Green dashed arrows in (d) and (f) are the paths used to calculate outflow speeds of the plasma. The x-axis of (a) is the same as (c). Animation of (c) is available online.

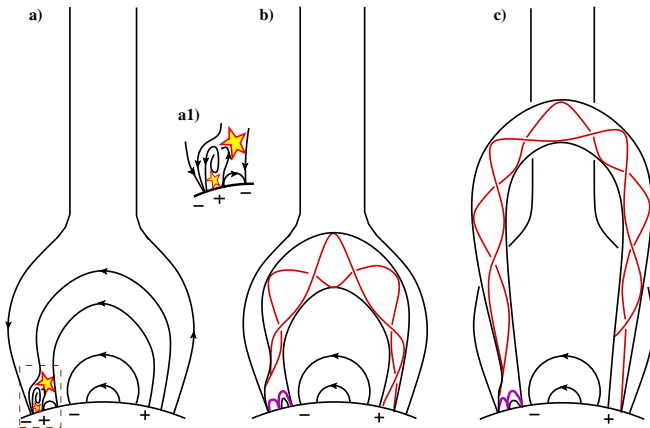


Figure 4. Schematic interpretation of the observations based on HMI, AIA, and LASCO images. These drawings depict the AR forming the helmet arcade below the streamer, viewed on the limb from the south. The helical black line in (a) represents twisted magnetic field in the jet base before and early during jet eruption. Stars show the locations where reconnection is taking place. Insert (a1) shows a zoomed-in view of the brown-boxed region of (a). The thick low magenta loops in (b) and (c) represent flare loops that result from internal (left) and external (right) reconnection of the erupting twisted field. (Complex flare loops at the jets' base in Figure 1 would correspond to the low-lying magenta loops of (b) and (c).) The red lines in (b) and (c) represent the twist transferred from the erupting field to the high-reaching jet-guiding coronal loop of the streamer-base helmet arcade by the external reconnection. The '+' and '-' labels are for positive and negative magnetic polarity, respectively.

also. Moreover, AIA images of our events here show no indication of an erupting plasmoid (which would appear as a largely-intact closed-loop flux-rope structure; see Figures 3(b) and 3(c) of Bemporad et al. (2005)). Rather, apparently the minifilament field is entirely opened by the external reconnection and ceases to be a plasmoid early in the jet-formation process (Figures 4(a), 4(a1) and 4(b)), having become new big-arch field in the jet and new closed loops in the jet's base (Figure 1(b, f, and j)). Therefore, at least for the events presented here, the Figure 4 schematic explains the streamer-puff phenomenon better than does the schematic of Bemporad et al. (2005).

This work was funded by the Heliophysics Division of NASA's Science Mission Directorate through the Living With a Star Targeted Research and Technology Program, and by the *Hinode* Project. N.K.P. is supported by an appointment to the

NASA Postdoctoral Program at the NASA MSFC, administered by USRA through a contract with NASA.

REFERENCES

- Archontis, V., & Hood, A. W. 2013, *ApJ*, 769, L21
 Bemporad, A., Sterling, A. C., Moore, R. L., & Poletto, G. 2005, *ApJ*, 635, L189
 Brueckner, G. E., Howard, R. A., Koomen, M. J., et al. 1995, *Sol. Phys.*, 162, 357
 Chen, H., Zhang, J., Ma, S., et al. 2015, *ApJ*, 808, L24
 Cirtain, J. W., Golub, L., Lundquist, L., et al. 2007, *Science*, 318, 1580
 Dodson-Prince, H. W., & Bruzek, A. 1977, *Illustrated Glossary for Solar and Solar-Terrestrial Physics*, ed. A. Bruzek & C. J. Durrant (Dordrecht: Springer Netherlands), 81–96
 Fang, F., Fan, Y., & McIntosh, S. W. 2014, *ApJ*, 789, L19
 Jiang, Y., Yang, J., Zheng, R., Bi, Y., & Yang, X. 2009, *ApJ*, 693, 1851
 Lemen, J. R., Title, A. M., Akin, D. J., et al. 2012, *Sol. Phys.*, 275, 17
 Li, X., Yang, S., Chen, H., Li, T., & Zhang, J. 2015, *ApJ*, 814, L13
 Lin, R. P., Dennis, B. R., Hurford, G. J., et al. 2002, *Sol. Phys.*, 210, 3
 Moore, R. L., Cirtain, J. W., Sterling, A. C., & Falconer, D. A. 2010, *ApJ*, 720, 757
 Moore, R. L., & Sterling, A. C. 2007, *ApJ*, 661, 543
 Moore, R. L., Sterling, A. C., & Falconer, D. A. 2015, *ApJ*, 806, 11
 Nisticò, G., Bothmer, V., Patsourakos, S., & Zimbardo, G. 2009, *Sol. Phys.*, 259, 87
 Panesar, N. K., Sterling, A. C., Innes, D. E., & Moore, R. L. 2015, *ApJ*, 811, 5
 Pariat, E., Antiochos, S. K., & DeVore, C. R. 2009, *ApJ*, 691, 61
 Scherrer, P. H., Schou, J., Bush, R. I., et al. 2012, *Sol. Phys.*, 275, 207
 Schou, J., Scherrer, P. H., Bush, R. I., et al. 2012, *Sol. Phys.*, 275, 229
 Sheeley, N. R., Walters, J. H., Wang, Y.-M., & Howard, R. A. 1999, *J. Geophys. Res.*, 104, 24739
 Sheeley, Jr., N. R., Lee, D. D.-H., Casto, K. P., Wang, Y.-M., & Rich, N. B. 2009, *ApJ*, 694, 1471
 Shibata, K., & Uchida, Y. 1986, *Sol. Phys.*, 103, 299
 Shibata, K., Ishido, Y., Acton, L. W., et al. 1992, *PASJ*, 44, L173
 Shimojo, M., Hashimoto, S., Shibata, K., et al. 1996, *PASJ*, 48, 123
 Sterling, A. C., & Moore, R. L. 2001, *J. Geophys. Res.*, 106, 25227
 Sterling, A. C., Moore, R. L., Falconer, D. A., & Adams, M. 2015, *Nature*, 523, 437
 Sun, X., Bobra, M. G., Hoeksema, J. T., et al. 2015, *ApJ*, 804, L28
 Tang, F., & Moore, R. L. 1982, *Sol. Phys.*, 77, 263
 Thalmann, J. K., Su, Y., Temmer, M., & Veronig, A. M. 2015, *ApJ*, 801, L23
 Török, T., Aulanier, G., Schmieder, B., Reeves, K. K., & Golub, L. 2009, *ApJ*, 704, 485
 Vourlidas, A., Lynch, B. J., Howard, R. A., & Li, Y. 2013, *Sol. Phys.*, 284, 179
 West, M. J., & Seaton, D. B. 2015, *ApJ*, 801, L6
 Yashiro, S., Gopalswamy, N., Michalek, G., et al. 2004, *Journal of Geophysical Research (Space Physics)*, 109, 7105
 Zirin, H. 1988, *Astrophysics of the sun*